J. Fluid Mech. (1982), *vol.* 122, *pp.* 91–108
Printed in Great Britain

Forced convection in a rapidly rotating annulus

By A. T. CONLISK

Department of Mechanical Engineering, The Ohio State University, Columbus, Ohio 43210

AND J. D. A. WALKER

Department of Mechanical Engineering and Mechanics, Lehigh University, Bethlehem, Pennsylvania

(Received 24 August 1981)

The source–sink flow within a rapidly rotating annular region, bounded by a pair of concentric circular cylinders and by horizontal end plates, is considered. Fluid is injected into the container at arbitrary locations on the inner radius and withdrawn at one or more locations on either the inner or outer radius, through axisymmetric slots. The upper end wall is maintained at a higher constant temperature than the bottom end plate, while the vertical side walls are thermally insulated; the entire apparatus is rapidly rotating about the common axis of the cylinders. An analysis of the flow and temperature distribution is carried out in the context of the Boussinesq approximation and by assuming that vertical buoyancy effects are negligible to leading order. A method for calculation of the temperature distribution within the container is developed for physical situations where the effects of the imposed thermal gradient and the source–sink flow are of comparable magnitudes; the procedure is applicable for an arbitrary distribution of sources and sinks on the side walls. The temperature problem is an unusual complicated boundary-value problem, and numerical solutions are obtained for a number of different cases. The results reveal a number of interesting flows and temperature fields within the container and indicate how the temperature field is influenced by the placement and temperature of the sources and sinks, as well as by the relative magnitudes of the imposed forced flow and vertical thermal gradient. The possible application of the present theory to centrifuges is indicated.

1. Introduction

There are a wide variety of geophysical and engineering applications associated with flows in a rapidly rotating container, and consequently fundamental problems associated with such flows have been of interest for a number of years. Three basic mechanisms for inducing motion within a rapidly rotating container have been examined in some detail in the literature. These are: (i) *differential rotation*, whereby one or more of either the side walls or end walls is rotated at a slightly different rate from the rest of the container (Stewartson 1957; Foster 1972); (ii) *an applied thermal gradient*, whereby an externally applied horizontal or vertical temperature gradient occurs (Hunter 1967; Barcilon & Pedlosky 1967; Homsy & Hudson 1969); and (iii) *an imposed source–sink flow*, whereby fluid is continually injected and withdrawn from the container (Hide 1968; Bennetts & Hocking 1973; Bennetts & Jackson 1974; Conlisk &

Walker 1981). In each of the cited investigations the motion due to a single effect is considered, and it emerges that, insofar as the induced geostrophic motion is concerned, the effects of an applied thermal gradient and differential rotation are similar. In many situations, two of these effects are present concurrently; for example, in a thermally driven gas centrifuge (Olander 1972), which is a device used to separate binary mixtures, a source–sink flow and a thermally induced flow occur. In the present study, a geometry similar to a typical gas centrifuge is considered; specifically, a rapidly rotating annular region that is bounded in the vertical direction by horizontal plates. The motion due to the combination of an applied vertical thermal gradient and a source–sink flow is investigated.

The general nature of source–sink flows in a rapidly rotating environment was established in an extensive series of experiments by Hide (1968). In the majority of these experiments, the fluid was contained radially by a pair of concentric cylinders and vertically by top and bottom end plates; fluid was uniformly injected at the inner cylinder and withdrawn along the outer wall. The basic structure of the flow field consists of an interior geostrophic region, Ekman boundary layers on the horizontal surfaces and a set of vertical shear layers having thicknesses $O(E^{\frac{1}{4}})$ and $O(E^{\frac{1}{3}})$; here E is the Ekman number. In the experiments, fluid entering at the inner radius was observed to be immediately deflected toward the Ekman layers and to traverse the container via the Ekman layers. At the outer wall, the fluid is deflected back into the shear layers before withdrawal from the container. There is no radial or vertical motion in the geostrophic core, but a circumferential velocity, in a direction opposite to that of the rotation, occurs. Conlisk & Walker (1981) have recently considered the case of injection and withdrawal through axisymmetric slots in the side walls; it was demonstrated that although the $E^{\frac{1}{3}}$ layer patterns can become very complicated, depending on the method of injection, only the flow in the $E^{\frac{1}{3}}$ layer is affected by the method of injection or withdrawal.

Relative motion within a rotating container may also be generated by imposing a temperature gradient. Barcilon & Pedlosky (1967) investigated the flow in a rapidly rotating cylindrical container due to a small imposed vertical temperature gradient, and analysed the case where buoyancy and centrifugal forces are comparable. In this situation, a small vertical drift velocity, proportional to the applied temperature gradient, is induced within the core; in addition, only a single $E^{\frac{1}{3}}$ shear layer is required to bring the thermally induced motion to relative rest on the side wall. The cylindrical wall of the container was taken to be thermally insulated, and solutions for the temperature field were obtained in two parameter ranges. The first of these corresponds to a diffusion-dominated regime, in which the temperature is independent of radius and varies linearly with vertical distance. The second parameter range is more difficult, and corresponds physically to a situation where convection and diffusion of heat are of comparable importance. It was determined that a thermal coupling occurs between the boundary layers and the core region; this is because energy that is convected into the vertical shear layers cannot be removed at the side walls and must be returned to the core. In this case the boundary conditions for the geostrophic temperature distribution are complicated, and Barcilon & Pedlosky (1967) approach the problem by considering small perturbations about the purely diffusive solution.

Homsy & Hudson (1969) investigate the same problem as Barcilon & Pedlosky, but concentrate on the case where the flow is dominated by centrifugal forces. The tem-

perature distribution in the case where diffusion and convection of heat are of comparable importance was computed numerically; these results show that the isotherms, which are horizontal for the purely diffusive case, are deflected in the local direction of the flow to an increasing extent as convection effects become progressively more important. Finally, Hunter (1967) considered a similar type of problem but with insulated end walls.

In this paper the objective is to obtain solutions for the flow field and temperature distribution for slightly compressible source–sink flow within a rapidly rotating annular region having insulated side walls and end plates maintained at constant temperatures; in this manner, the flow is exposed to a vertical thermal gradient. The analysis will be carried out in the context of the Boussinesq approximation (Spiegel & Veronis 1960); consequently, although the geometry is similar to that of some types of centrifuges, the results of the analysis are not strictly applicable to the highly compressed motion within a real gas centrifuge (Olander 1972). On the other hand, the analysis reveals the effects of the placement of the sources and sinks on the temperature distribution for a Boussinesq fluid and establishes the character of the combined thermal and source–sink induced flow. It is also of interest to note that the temperature problem involves a rather unusual and complex set of boundary conditions.

To fix the problem mathematically, consider an annular region of height L which is bounded by two concentric cylinders of radius aL and bL, where a and b are dimensionless and $b > a$. Fluid is injected into the container at one or more axisymmetric slots along the inner radius and withdrawn at one or more slots on the outer wall. The cylindrical side walls are thermally insulated; the fluid is confined in the vertical direction by upper and lower horizontal plates maintained at constant temperatures T_1^* and T_0^* respectively, where $T_1^* = T_0^* + \Delta T$ and $\Delta T > 0$. The entire apparatus is rapidly rotating with angular velocity Ω about the axis of the cylinders. Under these conditions, the flow field and temperature distribution are axisymmetric, and as a point of reference the geometrical configuration along with a typical source–sink geometry is depicted in figure 1.

If all lengths and velocities are made dimensionless with respect to the container depth L and a representative speed U_0, the equations governing the steady motion, written in a frame of reference which rotates uniformly with the apparatus, are

$$(1-\epsilon_T T)\,\epsilon_f(\mathbf{q}\cdot\nabla)\mathbf{q} + 2(1-\epsilon_T T)\,(\hat{\mathbf{i}}_z\times\mathbf{q}) = -\nabla p - E\nabla\times(\nabla\times\mathbf{q}) - \gamma r T\hat{\mathbf{i}}_r + (\gamma/Fr)\,T\hat{\mathbf{i}}_z, \tag{1.1}$$

$$\nabla\cdot\mathbf{q} = 0, \tag{1.2}$$

$$\epsilon_f Pr(\mathbf{q}\cdot\nabla T) = E\nabla^2 T. \tag{1.3}$$

Here (r,θ,z) are cylindrical co-ordinates having origin on the axis of rotation in the lower horizontal plate, and $\mathbf{q} = (u,v,w)$ is the velocity vector in the rotating frame; $\hat{\mathbf{i}}_r$ and $\hat{\mathbf{i}}_z$ are unit vectors in the r- and z-directions respectively; p and T are the reduced pressure and dimensionless temperature difference, defined according to

$$\frac{p^*}{\rho_0^*} = gz - \tfrac{1}{2}\Omega^2 r^2 + U_0\Omega L p, \quad T = \frac{T^* - T_0^*}{\Delta T}, \tag{1.4a, b}$$

where the asterisk denotes a dimensional quantity, p^* and T^* are the pressure and temperature respectively, and ρ_0^* is the density of the fluid at the lower plate. In (1.1)–(1.3) the five dimensionless parameters that govern the motion are the fluid

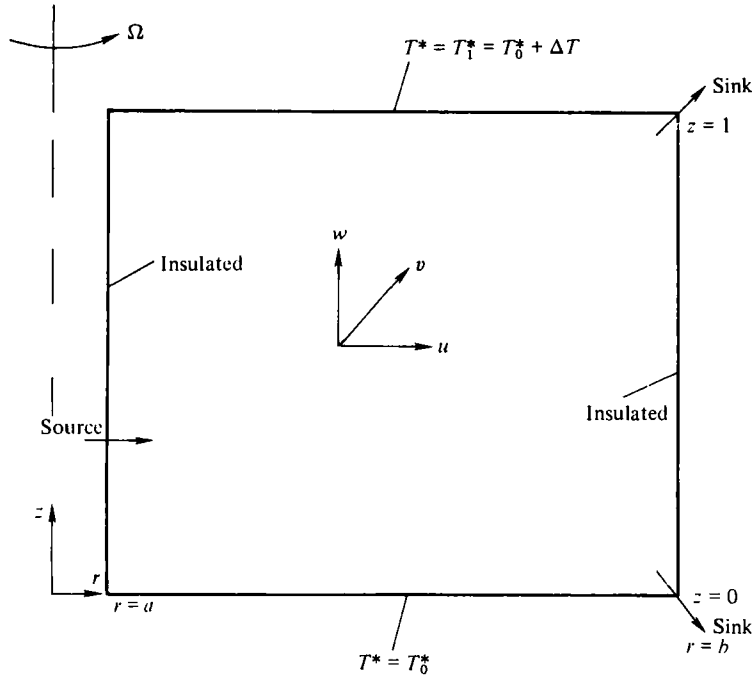

FIGURE 1. Geometry and co-ordinate system in cross-section. The arrows on the side walls denote possible locations for slots of injection or withdrawal of fluid. The flow in the annulus is due to a combination of a source–sink flow and a thermally driven flow induced by the imposed vertical temperature gradient.

Rossby number ϵ_f, the thermal Rossby number ϵ_T, the Prandtl number Pr, the Froude number Fr and the Ekman number E; these parameters are defined according to

$$\epsilon_f = \frac{U_0}{\Omega L}, \quad \epsilon_T = \alpha \Delta T, \quad Pr = \frac{\mu C_p}{k}, \quad Fr = \frac{\Omega^2 L}{g}, \quad E = \frac{\nu}{\Omega L^2}. \tag{1.5}$$

Here μ and ν are the absolute and kinematic viscosities respectively, C_p is the specific heat at constant pressure, $\alpha = 1/T_0^*$ is the coefficient of thermal expansion, k is the thermal conductivity and g is the gravitational acceleration. Finally, in (1.1), γ is the ratio of the Rossby numbers, defined according to

$$\gamma = \epsilon_T / \epsilon_f. \tag{1.6}$$

In this study it is assumed that Pr is $O(1)$ and that the flow is rapidly rotating in the sense that $E \ll 1$. It can be shown that the vertical-buoyancy term in (1.1) is negligible to leading order throughout the flow field provided that $Fr \gg E^{-\frac{1}{2}}$, and this condition is assumed. In addition, the physical situation of interest here corresponds to the case where the effects of the imposed source–sink and the thermally induced flow are comparable, and consequently it is assumed that $\epsilon_f = O(\epsilon_T)$, or equivalently that γ is $O(1)$. Within this framework, two parameter ranges are of interest here. For $\epsilon_f \ll E^{\frac{1}{2}}$, corresponding to very weak injection, it emerges that the convective terms in both the momentum and energy equation are negligible to leading order; in this case the geostrophic circumferential velocity and temperature distribution are readily computed (Conlisk 1978). For stronger rates of injection, corresponding to $\epsilon_f = O(E^{\frac{1}{2}})$, the

convective terms in the energy equation must be considered, and for the core temperature and velocity distribution there is a complex coupling between the vertical shear layers and the geostrophic flow. In §§2–4, this problem is formulated by consideration of the dynamics of the geostrophic region, the $E^{\frac{1}{4}}$ layer and the $E^{\frac{1}{3}}$ layers respectively. The temperature problem in this parameter range is a complicated and unusual nonlinear boundary-value problem, and numerical solutions are described in §5. The conclusions and relevant applications of the present study are described in §6.

2. The geostrophic flow

The geostrophic flow arises from the imposed source–sink flow as well as the applied thermal gradient; however, it may be verified that for $\epsilon_t \ll E^{\frac{1}{4}}$ (Bennetts & Hocking 1973) the leading-order fluid motion may be analysed on the basis of linear theory, and consequently both effects may be treated separately.

The total mass flow $\dot{m}^*$ through the container is in all cases assumed small and is given by

$$\dot{m}^* = 2\pi a L^2 \rho_0^* U_0 E^{\frac{1}{4}}. \tag{2.1}$$

Note that this equation may be considered as a definition of the representative speed U_0. All sources and sinks are assumed to be located on the side walls and the net mass flux is from the inner to the outer radius. Conlisk & Walker (1981) have recently given solutions for all possible methods of injection and withdrawal; in particular, using a subscript S to denote the source–sink generated motion, the geostrophic solution in all situations is given by

$$V_{\mathrm{GS}} = -a/r, \quad U_{\mathrm{GS}} = W_{\mathrm{GS}} = 0. \tag{2.2}$$

The geostrophic equations for the thermally induced motion follow from (1.1)–(1.3) and are

$$-2V_{\mathrm{GT}} = -\frac{\partial p_{\mathrm{GT}}}{\partial r} - \gamma r T_{\mathrm{G}}, \quad U_{\mathrm{GT}} = \frac{\partial p_{\mathrm{GT}}}{\partial z} = \frac{\partial W_{\mathrm{GT}}}{\partial z} = 0, \tag{2.3a, b}$$

where in (2.3) the subscripts G and T refer to geostrophic and thermally driven motion respectively. The Ekman compatibility conditions are

$$W_{\mathrm{GT}} = \pm \tfrac{1}{2} E^{\frac{1}{2}} \frac{\partial V_{\mathrm{GT}}}{\partial r} \quad \text{at} \quad z = \tfrac{1}{2} \mp \tfrac{1}{2}, \tag{2.4}$$

and in addition it can be shown readily that in general there is a radial flux outward in each Ekman layer equal to $-\frac{1}{2}E^{\frac{1}{2}}(U_{\mathrm{G}} + V_{\mathrm{G}})$ per unit length of circumference; in this case, since $U_{\mathrm{GT}} = 0$ and since there can be no net mass flux across a cylindrical control surface due to the thermally induced motion, it follows that

$$V_{\mathrm{GT}}(r, 1) + V_{\mathrm{GT}}(r, 0) = 0. \tag{2.5}$$

The boundary conditions at the end plates for the temperature distribution follow from (1.4*b*) as

$$T_{\mathrm{G}}(r, 0) = 0, \quad T_{\mathrm{G}}(r, 1) = 1. \tag{2.6}$$

Using (2.5) and (2.6) in (2.3) it follows that

$$\frac{dP_{\mathrm{GT}}}{dr} = -\tfrac{1}{2}\gamma r, \tag{2.7}$$

and from (2.4) that

$$W_{GT} = -\tfrac{1}{4}\gamma E^{\frac{1}{2}}. \tag{2.8}$$

Consequently the temperature gradient induces a weak vertical drift from the upper to the lower Ekman layer.

The circumferential velocity V_{GT} is related through the first of (2.3) to the temperature distribution T_G, which in turn satisfies

$$\frac{\partial^2 T_G}{\partial r^2} + \frac{1}{r}\frac{\partial T_G}{\partial r} + \frac{\partial^2 T_G}{\partial z^2} = \frac{-Pr\gamma\epsilon_f}{4E^{\frac{1}{2}}}\frac{\partial T_G}{\partial z}. \tag{2.9}$$

The solution of this equation depends upon the magnitude of ϵ_f, or equivalently, for $\gamma = O(1)$, on the magnitude of ϵ_T. For $\epsilon_f \ll E^{\frac{1}{2}}$, (2.9) becomes a Laplace equation, and the solution satisfying the insulated-side-wall conditions

$$\frac{\partial T_G}{\partial r} = 0 \quad \text{at} \quad r = a, b \tag{2.10}$$

is the diffusive solution

$$T_G = z. \tag{2.11}$$

In this case, it follows from (2.3a) that

$$V_{GT} = \tfrac{1}{2}\gamma r(z - \tfrac{1}{2}). \tag{2.12}$$

Note that this thermally induced swirl velocity is in the same direction as the rotation for $z > \frac{1}{2}$, and opposite to the rotation for $z < \frac{1}{2}$; the combination gives

$$V_G(r, z) = -\frac{a}{r} + \tfrac{1}{2}\gamma r(z - \tfrac{1}{2}).$$

Thus $V_G < 0$ in the lower portion of the annulus, and changes sign along the curve

$$z_c = \frac{1}{2}\left(1 + \frac{4a}{\gamma r^2}\right).$$

For $\epsilon_f = O(E^{\frac{1}{2}})$ the convective term on the right-hand side of (2.9) must be considered; in addition, the convective terms enter the energy equation to leading order in the vertical shear layers, and the side-wall conditions (2.10) are no longer appropriate. The determination of the correct geostrophic temperature boundary conditions at $r = a, b$ for $\epsilon_f = O(E^{\frac{1}{2}})$ is the objective of §§3 and 4. Note that in this case, once $T_G(r, z)$ is known, $V_{GT}(r, z)$ is obtained from (2.3a).

3. The $E^{\frac{1}{4}}$ layers

The swirl velocity $V_{GS} = -a/r$ is independent of z and may therefore be reduced to relative rest on the side walls by means of an $E^{\frac{1}{4}}$ layer. The thermally induced velocity V_{GT} in general depends on z, and an $E^{\frac{1}{2}}$ layer is required for the adjustment to relative rest on the walls. The $E^{\frac{1}{4}}$-layer velocities are given by (Conlisk & Walker 1981)

$$U_{\frac{1}{4}} = CE^{\frac{1}{4}}e^{-\xi}, \quad V_{\frac{1}{4}} = C(e^{-\xi} - 1), \quad W_{\frac{1}{4}} = \theta C\sqrt{2}\,E^{\frac{1}{4}}(z - \tfrac{1}{2})\,e^{-\xi}, \tag{3.1}$$

where

$$\xi = (r - a)\,E^{-\frac{1}{4}}, \quad \theta = 1, \quad C = 1 \quad \text{at} \quad r = a,$$

or

$$\xi = (b - r)\,E^{-\frac{1}{4}}, \quad \theta = -1, \quad C = a/b \quad \text{at} \quad r = b.$$

The convective terms in (1.3) become comparable to the diffusive terms when $\epsilon_f = O(E^{\frac{1}{4}})$, and thus we formally define

$$\epsilon_f = \lambda E^{\frac{1}{4}}.$$

The form of the temperature expansion in the $E^{\frac{1}{4}}$ layer is now determined by expansion of the geostrophic temperature for fixed z with $r \to \delta$, where δ denotes either a or b; accordingly, in the $E^{\frac{1}{4}}$ layer

$$T_{\frac{1}{4}} = T_G(\delta, z) + \theta E^{\frac{1}{4}} \left\{ \bar{T}_0(\xi, z) + \frac{\xi}{\sqrt{2}} \left. \frac{\partial T_G}{\partial r} \right|_{r=\delta} \right\} + \ldots, \tag{3.2}$$

where the equation for the correction is obtained by substitution of (3.1) and (3.2) into (1.3), and it follows that

$$\frac{\partial^2 \bar{T}_0}{\partial \xi^2} = -\lambda Pr C \tfrac{1}{2} \sqrt{2}\,(z - \tfrac{1}{2})\, e^{-\xi} \left. \frac{\partial T_G}{\partial z} \right|_{r=\delta}.$$

This equation may be integrated subject to the matching conditions that $\partial \bar{T}_0 / \partial \xi$, $\bar{T}_0 \to 0$ as $\xi \to \infty$. In particular, it is easily verified that

$$\left. \frac{\partial \bar{T}_0}{\partial \xi} \right|_{\xi=0} = -\lambda Pr\, C \tfrac{1}{2} \sqrt{2}\,(z - \tfrac{1}{2}) \left. \frac{\partial T_G}{\partial z} \right|_{r=\delta}. \tag{3.3}$$

It may be observed from (3.3) that the temperature solution does not satisfy the insulated-side-wall condition and is therefore not uniformly valid. An inner $E^{\frac{1}{3}}$ layer is required, and this is considered next.

4. The $E^{\frac{1}{3}}$ layers

The inner $E^{\frac{1}{3}}$ layers adjacent to the wall reduce the swirl velocity associated with the thermally induced motion to relative rest, contain the structure of the source–sink flow, and adjust the temperature field to the insulated boundary conditions. In the $E^{\frac{1}{3}}$ layer, the expansions for the velocity components are written as

$$v_{\frac{1}{3}} = V_{GT}(\delta, z) + v_{0T}(\eta, z) - \sqrt{2}\, C\eta\, E^{\frac{1}{12}} + E^{\frac{1}{3}} \{ v_{2S}(\eta, z) + v_{2T}(\eta, z) \} + \ldots, \tag{4.1}$$

$$w_{\frac{1}{3}} = \theta w_{0T}(\eta, z) + \theta E^{\frac{1}{3}} \{ w_{2S}(\eta, z) + w_{2T}(\eta, z) \} + \ldots, \tag{4.2}$$

$$u_{\frac{1}{3}} = E^{\frac{1}{3}} u_{0T}(\eta, z) + E^{\frac{1}{3}} \{ u_{2S}(\eta, z) + u_{2T}(\eta, z) \} + \ldots, \tag{4.3}$$

where η is the scaled variable in the $E^{\frac{1}{3}}$ layer and $\eta = \theta(r - \delta) E^{-\frac{1}{3}}$. Here again δ denotes either a or b, and $\theta = \pm 1$ at $r = a$ and b respectively. Note that $V_{GT}(\delta, z)$ is the, as yet, undetermined thermally induced geostrophic swirl velocity evaluated as $r \to \delta$; furthermore, the subscripts S and T are also used here to denote source–sink and thermally induced motion respectively.

Upon substitution of the expansions (4.1)–(4.3) into (1.1) it is readily shown that the lowest-order terms satisfy the usual $E^{\frac{1}{3}}$-layer equations,

$$\frac{\partial^3 v_{0T}}{\partial \eta^3} = -2 \frac{\partial w_{0T}}{\partial z}, \quad \frac{\partial^3 w_{0T}}{\partial \eta^3} = 2 \frac{\partial u_{0T}}{\partial z}, \quad \frac{\partial u_{0T}}{\partial \eta} + \frac{\partial w_{0T}}{\partial z} = 0, \tag{4.4}$$

with the boundary conditions

$$w_{0T}, u_{0T}, v_{0T} \to 0 \quad \text{as} \quad \eta \to \infty, \tag{4.5}$$

$$u_{0T} = w_{0T} = 0, \quad v_{0T} = -V_{GT}(\delta, z) \quad \text{at} \quad \eta = 0, \tag{4.6}$$

and the Ekman condition

$$w_{0T} = 0 \quad \text{at} \quad z = 0, 1.$$

The solution is easily obtained as a Fourier series, and is

$$u_{0T} = \sum_{n=1}^{\infty} \frac{n\pi A_n}{\omega_n} \{e^{-\omega_n \eta} - e^{-\frac{1}{2}\omega_n \eta} \cos(\tfrac{1}{2}\sqrt{3}\,\omega_n \eta) + \sqrt{\tfrac{1}{3}}\, e^{-\frac{1}{2}\omega_n \eta} \sin(\tfrac{1}{2}\sqrt{3}\,\omega_n \eta)\} \cos n\pi z, \tag{4.7}$$

$$w_{0T} = \sum_{n=1}^{\infty} A_n \{e^{-\omega_n \eta} - e^{-\frac{1}{2}\omega_n \eta} \cos(\tfrac{1}{2}\sqrt{3}\,\omega_n \eta) - \sqrt{\tfrac{1}{3}}\, e^{-\frac{1}{2}\omega_n \eta} \sin(\tfrac{1}{2}\sqrt{3}\,\omega_n \eta)\} \sin n\pi z, \tag{4.8}$$

$$v_{0T} = \sum_{n=1}^{\infty} A_n \{e^{-\omega_n \eta} + e^{-\frac{1}{2}\omega_n \eta} \cos(\tfrac{1}{2}\sqrt{3}\,\omega_n \eta) + \sqrt{\tfrac{1}{3}}\, e^{-\frac{1}{2}\omega_n \eta} \sin(\tfrac{1}{2}\sqrt{3}\,\omega_n \eta)\} \cos n\pi z, \tag{4.9}$$

where $\omega_n = (4n\pi)^{\frac{1}{2}}$, and the Fourier coefficient A_n is given by

$$A_n = -\int_0^1 V_{GT}(\delta, z) \cos(n\pi z)\, dz. \tag{4.10}$$

In the linear case corresponding to $\epsilon_f \ll E^{\frac{1}{2}}$ ($\lambda = 0$), V_{GT} is known at this stage in the analysis and is given by (2.12); in this case it follows that

$$\begin{aligned} A_n &= \gamma\delta/n^2\pi^2 \quad (n \text{ odd}), \\ &= 0 \qquad\quad (n \text{ even}). \end{aligned}$$

However, for $\epsilon_f = O(E^{\frac{1}{2}})$, $V_{GT}(\delta, z)$ and thus the A_n are not yet determined. It is convenient at this point to express the A_n in terms of T_G; to this end, (2.3a) with (2.7) may be substituted in (4.10), and it may be shown that

$$A_n = -\tfrac{1}{2}\gamma\delta \int_0^1 T_G(\delta, z) \cos n\pi z\, dz. \tag{4.11}$$

A final comment with regard to this leading-order $E^{\frac{1}{2}}$ layer flow is that this thermally induced motion is purely recirculatory since

$$\int_0^\infty w_{0T}(\eta, z)\, d\eta = 0 \tag{4.12}$$

for all z and independent of the ultimate values of A_n.

The solution for the source–sink induced motion, u_{2S}, v_{2S} and w_{2S} in (4.1)–(4.3), depends on the method of injection and withdrawal from the container. It is assumed in this study that injection takes place through axisymmetric slots in the inner side wall which have a height $O(E^{\frac{1}{2}})$. Withdrawal is also assumed to take place through analogous slots on the outer periphery. The $E^{\frac{1}{2}}$-layer solutions for all possible modes of injection at the side wall have been considered by Conlisk & Walker (1981), and the results for w_{2S} will be utilized at a later stage in the analysis. The solution for the thermally induced motion, u_{2T}, v_{2T} and w_{2T}, depends on the temperature field, and this aspect is considered next.

In the $E^{\frac{1}{2}}$ layer, the expansion for the temperature field is written

$$\begin{aligned} T_{\frac{1}{2}} = {} & T_G(\delta, z) + \theta E^{\frac{1}{2}} T_1(\eta, z) + \theta E^{\frac{1}{2}} \bar{T}_0(0, z) \\ & + \theta E^{\frac{1}{2}} \left\{ T_2(\eta, z) + \sqrt{2}\,\eta \frac{\partial \bar{T}_0}{\partial \xi}(0, z) + \eta \left.\frac{\partial T_G}{\partial r}\right|_{r=\delta} \right\} + \ldots. \end{aligned} \tag{4.13}$$

In this expansion the term $O(E^{\frac{1}{2}})$ arises to balance a convective term of corresponding magnitude on the left-hand side of (1.3); in addition, $\bar{T}_0$ is the $E^{\frac{1}{2}}$-layer temperature perturbation in (3.2). Upon substitution of (4.1)–(4.3) and (4.13) in (1.3) it follows that

$$\frac{\partial^2 T_1}{\partial \eta^2} = \lambda Pr\, w_{0T} \frac{\partial T_G}{\partial z}\bigg|_{r=\delta},$$

and integration yields

$$\frac{\partial T_1}{\partial \eta} = -\lambda Pr \frac{\partial T_G}{\partial z}\bigg|_{r=\delta} \int_\eta^\infty w_{0T}\, d\eta. \tag{4.14}$$

Note that in view of (4.12) it follows that

$$\frac{\partial T_1}{\partial \eta} = 0 \quad \text{at} \quad \eta = 0. \tag{4.15}$$

A further integration of (4.14) and subsequent interchange of the order of integration leads to the solution

$$T_1(\eta, z) = \lambda Pr \frac{\partial T_G}{\partial z}\bigg|_{r=\delta} \int_\eta^\infty (t-\eta)\, w_{0T}(t, z)\, dt. \tag{4.16}$$

The integral in (4.16) may be evaluated using (4.8) in terms of the as yet unknown Fourier coefficients as defined by (4.10); however, the details are tedious and are omitted here.

The solution for the thermally induced flow $O(E^{\frac{1}{2}})$ may now be considered; this motion is important in the sense that it transports a flux of fluid $O(E^{\frac{1}{2}})$ on the side walls between the upper and the lower Ekman layers; on the outer wall this flux is upward, while it is downward on the inner wall. Equations for v_{2T} and w_{2T} may be obtained upon substitution of the expansions (4.1)–(4.3) and (4.13) into (1.1) and (1.2). Upon elimination of the pressure terms, it may be shown that

$$\frac{\partial^3 w_{2T}}{\partial \eta^3} - 2\frac{\partial v_{2T}}{\partial z} = \lambda\theta \frac{\partial}{\partial \eta}\left\{u_{0T}\frac{\partial w_{0T}}{\partial \eta} + w_{0T}\frac{\partial w_{0T}}{\partial z}\right\} - \gamma\delta\theta T_1(\eta, z), \tag{4.17a}$$

$$\frac{\partial^3 v_{2T}}{\partial \eta^3} + 2\frac{\partial w_{2T}}{\partial z} = \lambda\theta \frac{\partial}{\partial \eta}\left\{u_{0T}\frac{\partial v_{0T}}{\partial \eta} + w_{0T}\frac{\partial v_{0T}}{\partial z}\right\}. \tag{4.17b}$$

The Ekman conditions require that

$$w_{2T}(\eta, 0) = \frac{1}{2}\frac{\partial v_{0T}}{\partial \eta}\bigg|_{z=0} = F_0(\eta), \tag{4.18a}$$

$$w_{2T}(\eta, 1) = -\frac{1}{2}\frac{\partial v_{0T}}{\partial \eta}\bigg|_{z=1} = F_1(\eta), \tag{4.18b}$$

where the functions F_0 and F_1 may be readily obtained by using (4.9) and (4.10); note that both functions obtained this way are series containing the Fourier coefficients A_n. The equations are the usual $E^{\frac{1}{2}}$-layer equations apart from the forcing functions arising from the thermally induced leading-order recirculation and temperature distribution in the $E^{\frac{1}{2}}$ layer. In general, the solution of (4.17), with conditions (4.18) at $z = 0$ and 1 and with $u_{2T} = v_{2T} = w_{2T} = 0$ at $\eta = 0$ and as $\eta \to \infty$, is required. This boundary-value problem may be solved (in terms of the Fourier coefficients A_n) by standard methods; however, the algebraic details are involved, and the principal result for w_{2T} that is required in the subsequent analysis may be determined without

explicitly solving (4.17). This result concerns the vertical flux of fluid in each $E^{\frac{1}{3}}$ layer arising from the w_{2T} solution, and will be considered next.

It follows from (2.3), (2.6) and (2.7) that in general $V_{GT} = \pm \frac{1}{4}\gamma r$ at $z = 0$ and 1 respectively; consequently since $U_{GT} = 0$ to leading order, there is a net radial flux outward equal to $\pm \frac{1}{8}\gamma E^{\frac{1}{3}}$ in the bottom and top Ekman layers respectively, per unit length of circumference. This thermally induced flux enters or leaves the $E^{\frac{1}{3}}$ layer through the Ekman extensions of the $E^{\frac{1}{3}}$ layer, as may be readily verified by integration of (4.18) across the $E^{\frac{1}{3}}$ layer. Since $u_{2T} \to 0$, as $\eta \to \infty$, this flux is constant at any height z. Thus there is a thermally induced flux upward and equal to $\frac{1}{8}\gamma b E^{\frac{1}{3}}$ on the outer wall in the $E^{\frac{1}{3}}$ layer per unit length of circumference; there is a corresponding downward flux equal to $\frac{1}{8}\gamma a E^{\frac{1}{3}}$ on the inner wall. Consequently

$$\int_0^\infty w_{2T}(\eta, z)\, d\eta = -\tfrac{1}{8}\gamma\delta, \tag{4.19}$$

where again $\delta = a$ and b.

To complete the description of the temperature field in (4.13) through terms $O(E^{\frac{1}{3}})$, (4.2), (4.3) and (4.13) are substituted in (1.3), and it may be shown that

$$\frac{\partial^2 T_2}{\partial \eta^2} = \lambda Pr\,\theta\left\{u_{0T}\frac{\partial T_1}{\partial \eta} + w_{0T}\frac{\partial T_1}{\partial z}\right\} + \lambda Pr\,(w_{2S} + w_{2T})\left.\frac{\partial T_G}{\partial z}\right|_{r=\delta}. \tag{4.20}$$

Upon substitution of (4.16), (4.20) may be integrated once, and evaluation of this expression at $\eta = 0$ yields

$$\left.\frac{\partial T_2}{\partial \eta}\right|_{\eta=0} = -\lambda^2 Pr^2\theta\left.\frac{\partial T_G}{\partial z}\right|_{r=\delta}\beta_1(z) - \lambda^2 Pr^2\theta\left.\frac{\partial^2 T_G}{\partial z^2}\right|_{r=\delta}\beta_2(z) - \lambda Pr\left.\frac{\partial T_G}{\partial z}\right|_{r=\delta}\int_0^\infty (w_{2S} + w_{2T})\, d\eta, \tag{4.21}$$

where β_1 and β_2 are given by

$$\beta_1(z) = \int_0^\infty \int_s^\infty \{w_{0T}(s, z)\, u_{0T}(t, z) - w_{0T}(t, z)\, u_{0T}(s, z)\}\, dt\, ds,$$

$$\beta_2(z) = \int_0^\infty w_{0T}(s, z) \int_s^\infty (t - s)\, w_{0T}(t, z)\, dt\, ds.$$

These integrals may be evaluated upon substitution of (4.7) and (4.8), in terms of the Fourier coefficients A_n defined by (4.10); the results are

$$\left.\begin{aligned} \beta_1(z) &= -4\pi \sum_{n=1}^{\infty}\sum_{m=1}^{\infty} n\, A_m A_n g(m, n) \sin m\pi z \cos n\pi z, \\ \beta_2(z) &= -2 \sum_{n=1}^{\infty}\sum_{m=1}^{\infty} A_n A_m g(m, n) \sin n\pi z \sin m\pi z, \end{aligned}\right\} \tag{4.22}$$

where

$$g(m, n) = \frac{\omega_n \omega_m}{(\omega_m + \omega_n)(\omega_m^4 + \omega_n^4 + \omega_m^2\omega_n^2)}. \tag{4.23}$$

The last integral in (4.21) is given by (4.19). We define

$$\mathscr{F}_{\frac{1}{3}}(z) = \int_0^\infty w_{2S}(\eta, z)\, d\eta, \tag{4.24}$$

which represents the dimensionless flux in the $E^{\frac{1}{3}}$ layer associated with the $O(E^{\frac{1}{3}})$ flux due to the source–sink flow. The value of $\mathscr{F}_{\frac{1}{3}}$ will depend on the mode of injection or

withdrawal, and may be evaluated from the results of Conlisk & Walker (1981). Two cases are of interest here. First consider an axisymmetric slot having width $O(E^{\frac{1}{2}})$ and located on the side wall at $z = \Phi$; on the scale of the $E^{\frac{1}{3}}$ layer the slot appears as either a point source or sink, and it can be shown (Conlisk & Walker 1981) that

$$\mathscr{F}_{\frac{1}{3}} = \begin{matrix} C(1-z) & (z > \Phi) \\ -Cz & (z < \Phi) \end{matrix}, \tag{4.25}$$

where C is defined in connection with (3.1). Note that (4.25) holds for either a source on the inner wall or a sink on the outer wall at $z = \Phi$.

Another case of interest is that for sources located in the corner regions on the inner wall; in this case it may be shown (Conlisk & Walker 1981) that

$$\mathscr{F}_{\frac{1}{3}} = C(1-z) - C'z, \tag{4.26}$$

where C and C' denote the dimensionless strengths of each source at $z = 0$ and $z = 1$ respectively, and

$$C + C' = 1, \tag{4.27}$$

so that the total mass flux is given by (2.1). For sinks in the corner regions on the outer wall, of relative strengths $\hat{C}$ and $\hat{C}'$ at $z = 0$ and 1 respectively, the dimensionless flux is given by

$$\mathscr{F}_{\frac{1}{3}} = \hat{C}(1-z) - \hat{C}'z, \tag{4.28}$$

where

$$\hat{C} + \hat{C}' = a/b.$$

The flux due to other configurations may readily be constructed using the results of Conlisk & Walker (1981).

The boundary conditions at the side walls for the geostrophic temperature distribution $T_{\mathrm{G}}(r, z)$ may now be obtained by setting the derivative with respect to r of the expansion (4.13) equal to zero at $r = \delta$. Using (3.3) and (4.21), it may be shown that

$$\frac{\partial T_{\mathrm{G}}}{\partial r} + \lambda Pr f_1(z) \frac{\partial T_{\mathrm{G}}}{\partial z} + \lambda^2 Pr^2 f_2(z) \frac{\partial^2 T_{\mathrm{G}}}{\partial z^2} = 0 \tag{4.29}$$

at $r = \delta$, where

$$f_1(z) = -C(z - \tfrac{1}{2}) - \lambda Pr\, \theta \beta_1(z) - \mathscr{F}_{\frac{1}{3}} + \tfrac{1}{8}\gamma\delta\theta, \tag{4.30a}$$

$$f_2(z) = -\theta\beta_2(z). \tag{4.30b}$$

The solution of (2.9) for the geostrophic temperature distribution is now required subject to the boundary conditions (4.29) at $r = \delta$ ($\delta = a$ or b) and conditions (2.6) at $z = 0, 1$, for $\epsilon_{\mathrm{f}} = \lambda E^{\frac{1}{2}}$. Note that although (2.9) is linear, the boundary conditions (4.29) are highly nonlinear; this is due to the fact that the terms β_1 and β_2 in (4.30) consist of the double sums defined in (4.22). These sums contain the Fourier coefficients A_n defined in (4.11) in terms of T_{G}. Because of the unusual and nonlinear form of the boundary conditions in (4.29) an analytic solution could not be obtained, and the problem was solved numerically; the method is described in §5.

5. Calculated results

The problem defined by (2.6), (2.9) and (4.29) was solved numerically using finite-difference techniques. A square mesh with a uniform mesh length h in both the r- and z-directions was used in all calculations. At each internal mesh point, (2.9) was discretized using standard central-difference approximations; this procedure leads to a set of linear difference equations at each internal mesh point which may be solved by successive over-relaxation once an estimate of the solution on the boundary is available.

The treatment of the boundary condition (4.29) merits some discussion. Consider for example a typical point on the boundary at $r = a$ as depicted in figure 2. It was anticipated that variations in the radial direction would be more intense than in the vertical direction; in addition, to avoid introducing points outside the solution domain, a relatively accurate sloping-difference formula was used for the radial derivative. Referring to figure 2, the formula used (Abramowitz & Stegun 1965) is

$$h\frac{\partial T}{\partial r}\bigg|_1 = \tfrac{1}{6}\{-11T_1 + 18T_4 - 9T_5 + 2T_6\} + O(h^4). \tag{5.1}$$

The z-derivatives were approximated using standard central-difference formulae at the point 1. This procedure leads to a tridiagonal matrix problem for the temperature distribution along $r = a$, assuming that an estimate of the interior temperature distribution is available; a similar problem may be formulated on $r = b$.

The solution procedure is iterative, and is initiated by making an initial guess for T_G at all mesh points. The Fourier coefficients in (4.11) were then calculated using a Filon quadrature method (Abramowitz & Stegun 1965), and values of β_1 and β_2 were obtained by computing the sums in (4.22) at each mesh point on $r = a$ and $r = b$. Next a revised estimate of the temperature distribution on $r = a$ and $r = b$ was obtained by solving the tridiagonal problem along the boundary using a direct method and by holding the temperature values in the interior fixed. The first iteration was completed by revising the interior temperature distribution using successive over-relaxation with an over-relaxation factor of $\omega = 1{\cdot}75$. This process was continued until it converged, which was considered to have occurred when two successive iterates for the interior temperature values agreed to within four significant figures at each internal mesh point. Typically on the order of two hundred iterations were required.

For all cases considered, the Prandtl number Pr was set equal to unity, and the inner and outer radii were selected according to $a = 1$, $b = 2$; with $\epsilon_f = \lambda E^{\frac{1}{2}}$ and $\epsilon_T/\epsilon_f = \gamma$, various combinations of λ and γ were considered. In each case, a calculation was carried out with 11, 21 and 41 mesh points in each co-ordinate direction as a check on the accuracy. Close agreement between successive solutions is most difficult to achieve near the source and in the corner regions where the solution for T_G is believed to be irregular. Consider for example the case of a source on the inner wall; the inlet temperature T_S must be specified corresponding to the fluid entering the annulus at a fixed temperature T_S. The temperature along the inner wall is strongly influenced by the imposed vertical temperature gradient and also by thermal convection for $\epsilon_f = O(E^{\frac{1}{2}})$; when fluid enters at a temperature which is significantly different from that which would normally occur at that vertical location, the source appears as either a point source or point sink of heat. For such cases, the temperature solution will be

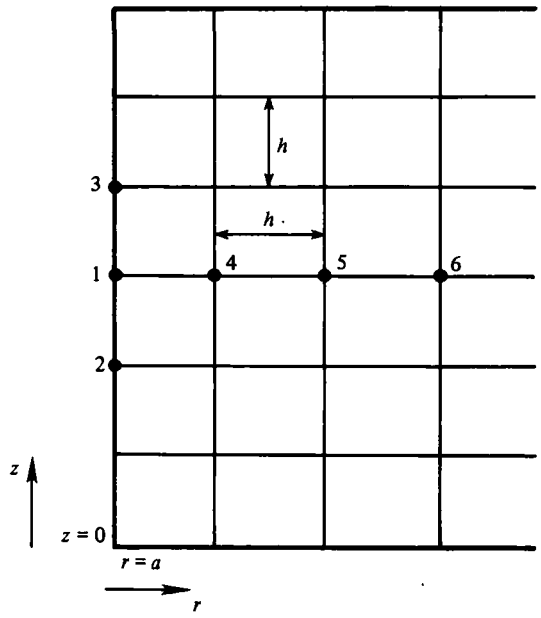

FIGURE 2. Notation for the finite-difference approximation to the radial and vertical derivatives at a typical vertical boundary. The approximation to the radial derivative is given in (5.1).

n	$A_n(r = a)$	Linear	$A_n(r = b)$	Linear
1	0·0895	0·1013	0·2231	0·2026
2	−0·0037	0	0·0173	0
3	0·0212	0·0113	0·0268	0·0226
4	0·0053	0	0·0059	0
5	0·0087	0·0041	0·0100	0·0082
6	−0·0004	0	0·0030	0
7	0·0022	0·0021	0·0053	0·0042
8	−0·0005	0	0·0019	0
9	0·0031	0·00125	0·0033	0·0025
10	0·0015	0	0·0013	0

TABLE 1. Coefficients A_n given by (4.11) on $r = a, b$ for $\lambda = \gamma = 1$, $T_s = 0{\cdot}5$. The source–sink geometry corresponds to a source at $z = 0{\cdot}3$ of strength 1 with two sinks of equal strength at $z = 0, 1$ on $r = b$. The linear coefficients ($\lambda = \gamma = 0$) are also shown.

irregular near the source and extreme accuracy of the numerical solution near such locations is precluded; agreement in successive numerical solutions was generally limited to two significant figures near sources and in the corner regions.

One important parameter in the calculations is the number n_0 of terms that are retained in computing the series in (4.22) for $\beta_1(z)$ and $\beta_2(z)$. Generally, for a given set of physical parameters, n_0 must be increased until no significant change in the solution occurs. However, as either λ or γ are increased the number of terms retained in (4.22) must be increased substantially, and this inevitably leads to relatively large computing times. As an example of the magnitudes of the coefficients in (4.11), a comparison is made in table 1 between a nonlinear case ($\lambda = \gamma = 1$) and the corresponding linear problem for A_n on $r = a$ and $r = b$.

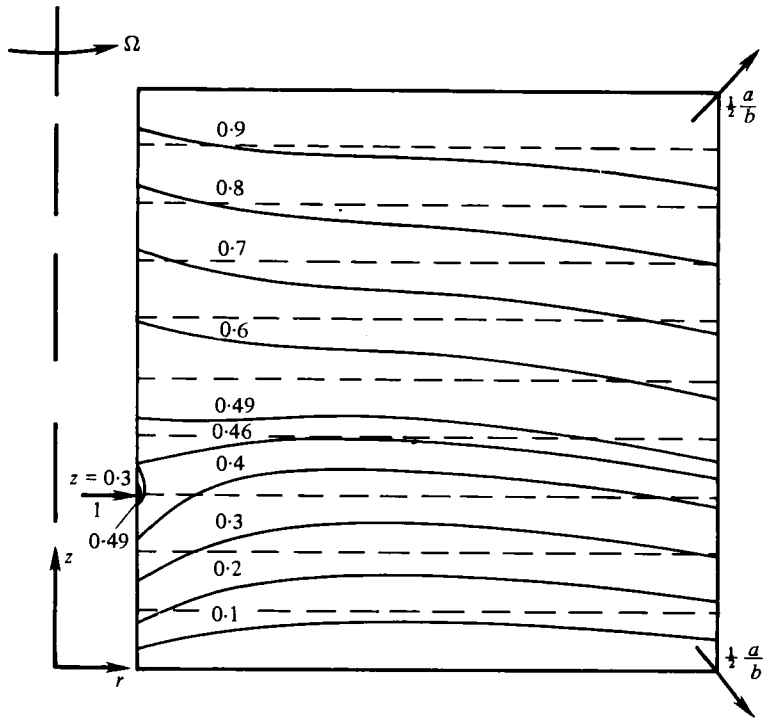

FIGURE 3. Isotherm patterns corresponding to the numerical solution of (2.9) for the geostrophic core-temperature distribution. The strengths of the sources and sinks are shown; here fluid enters at $z = 0{\cdot}3$ and is withdrawn through equal-strength sinks in the corners on $r = b$. On this figure $\lambda = 1, \gamma = 1$ and the temperature at the source $T_S = 0{\cdot}5$. Fluid is assumed to leave the container on $r = b$ at the end-wall temperatures. The dashed lines in this figure correspond to the linear solution for $\lambda, \gamma \ll 1$, $T = z$; here $a = 1, b = 2$. The dividing isotherm is 0·46.

Isotherms for a number of example cases are plotted in figures 3–7. In figure 3, the solution for the case $\gamma = \lambda = 1$ is depicted for a locally 'hot' source located at $z = 0{\cdot}3$ with $T_S = 0{\cdot}5$; note the source-like level curves near the entrance port on $r = a$ with the limiting isotherm near the source having the value 0·46. The dashed lines on the figure correspond to the purely diffusive solution $T_G = z$ which is valid in the linear case ($\lambda, \gamma \ll 1$). The effect of thermal convection near the side wall $r = b$ is to drive the isotherms downward in a direction opposite to the thermally induced upward motion in the $E^{\frac{1}{3}}$ layer. The distortion of the isotherms on the inner wall is a deflection away from the hot source. In figure 4, the effect of an increased flow rate is illustrated; the source–sink geometry, the source temperature and imposed temperature gradient ($\gamma = 1$) are identical with that adopted in figure 3, but now $\lambda = 3$. It may be observed that the effect is to increase the deflection of the isotherms. In figure 5, the effect of an increase in the temperature of the incoming fluid is illustrated for the same source–sink geometry, flow rate ($\lambda = 1$) and heating ($\gamma = 1$), but with $T_S = 0{\cdot}8$; the substantial distortion of the isotherms near the source should be noted. In figure 6, the effect of an increased level of differential heating ($\gamma = 3$) is illustrated for the same source–sink geometry.

As a final example, the effect of source–sink placement is illustrated in figure 7, where a source of strength $C = 1{\cdot}5$ is placed at $z = 0{\cdot}3$ and $r = a$; sinks of strength

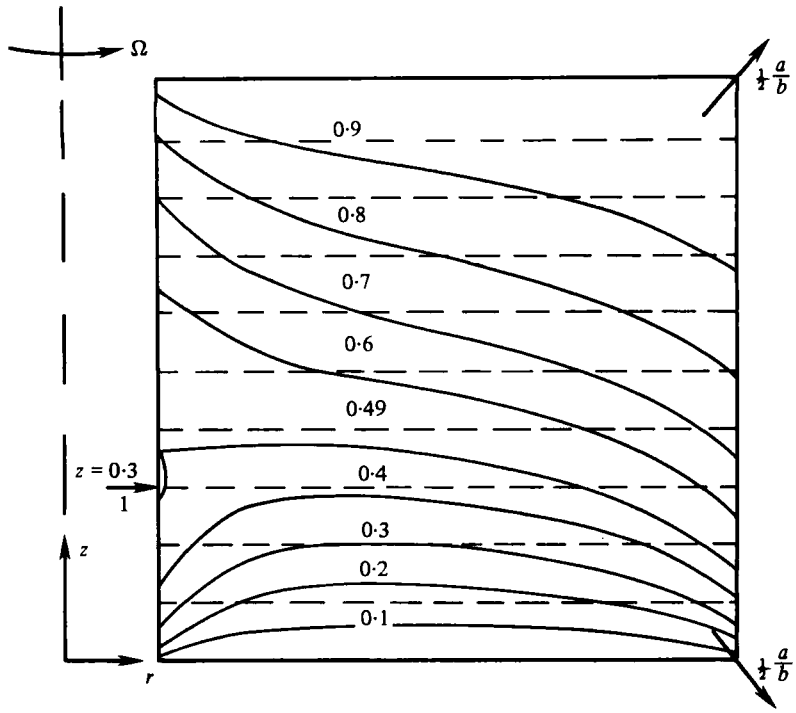

FIGURE 4. Isotherm patterns corresponding to the numerical solution of (2.9) for the geostrophic core-temperature distribution. The strengths of the sources and sinks are shown; here fluid enters at $z = 0{\cdot}3$ and is withdrawn through equal-strength sinks in the corners on $r = b$. On this figure $\lambda = 3$, $\gamma = 1$ and the temperature at the source $T_s = 0{\cdot}5$. Fluid is assumed to leave the container on $r = b$ at the end-wall temperatures. The dashed lines in this figure correspond to the linear solution for $\lambda, \gamma \ll 1$, $T = z$; here $a = 1$, $b = 2$. The dividing isotherm is 0·49.

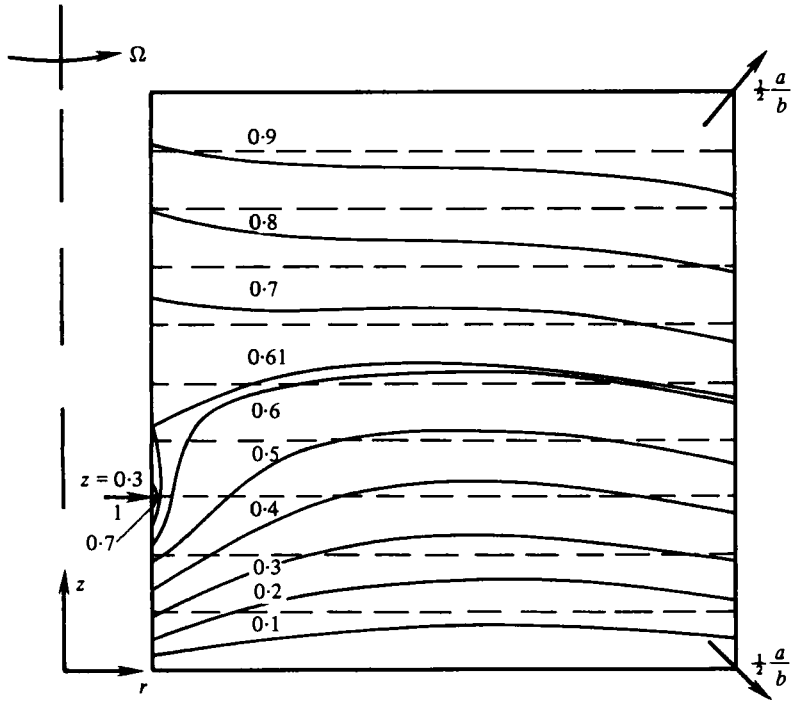

FIGURE 5. Isotherm patterns corresponding to the numerical solution of (2.9) for the geostrophic core-temperature distribution. The strengths of the sources and sinks are shown; here fluid enters at $z = 0{\cdot}3$ and is withdrawn through equal-strength sinks in the corners on $r = b$. On this figure $\lambda = 1$, $\gamma = 1$ and the temperature at the source $T_s = 0{\cdot}8$. Fluid is assumed to leave the container on $r = b$ at the end-wall temperatures. The dashed lines in this figure correspond

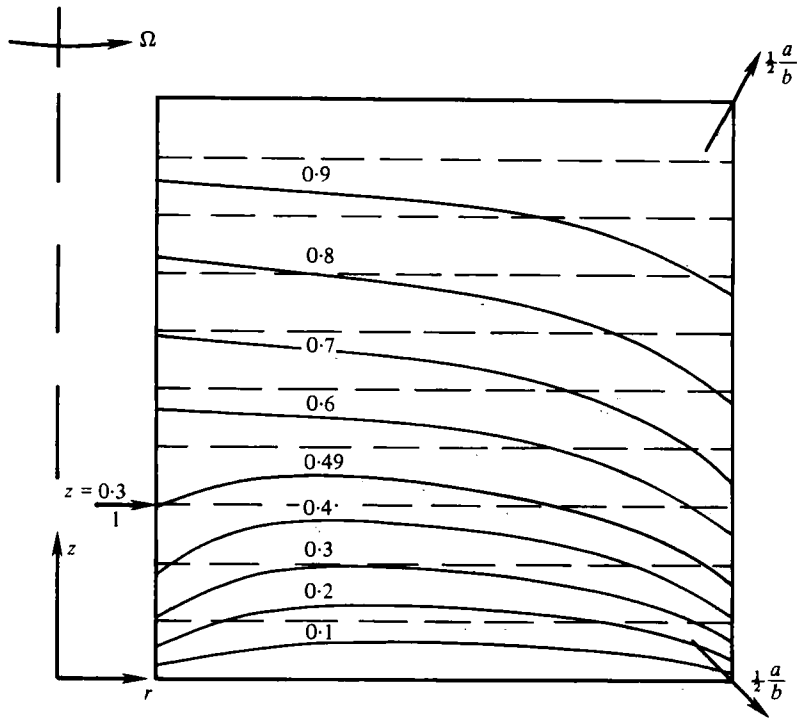

FIGURE 6. Isotherm patterns corresponding to the numerical solution of (2.9) for the geostrophic core-temperature distribution. The strengths of the sources and sinks are shown; here fluid enters at $z = 0{\cdot}3$ and is withdrawn through equal-strength sinks in the corners on $r = b$. On this figure $\lambda = 1, \gamma = 3$ and the temperature at the source $T_s = 0{\cdot}5$. Fluid is assumed to leave the container on $r = b$ at the end-wall temperatures. The dashed lines in this figure correspond to the linear solution for $\lambda, \gamma \ll 1$, $T = z$; here $a = 1, b = 2$.

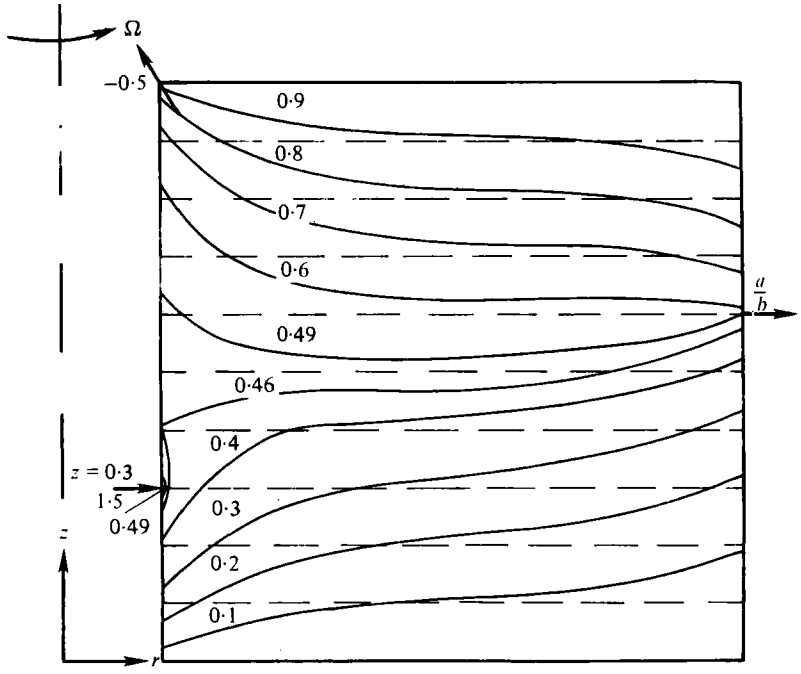

FIGURE 7. Isotherm patterns corresponding to the numerical solution of (2.9) for the geostrophic core-temperature distribution. The strength of the sources and sinks are shown; here fluid enters the container at $z = 0{\cdot}3$ and is withdrawn at $z = 1, r = a$ and at $z = 0{\cdot}6, r = b$. On this figure $\lambda = 2, \gamma = 0$ and the temperature at the source $T_s = 0{\cdot}5$. Fluid leaves on $r = a, z = 1$ at the end-wall temperature; the temperature at the sink $r = b, z = 0{\cdot}6$ is $T_{sink} = 0{\cdot}4$. The

$-0{\cdot}5$ and a/b are placed at $r = a$, $z = 1$ and $r = b$, $z = 0{\cdot}6$ respectively. The temperature of the source is $T_S = 0{\cdot}5$, while the sink temperature on $r = b$ is taken to be $T_{sink} = 0{\cdot}4$. In this case, $\lambda = 2$ and $\gamma = 0$ ($\epsilon_T \ll E^{\frac{1}{2}}$), and consequently the temperature distribution is determined entirely by forced convection. Note the bending of the isotherms near the sinks in the direction of the local forced flow. The source–sink geometry in this figure is similar to that used in actual gas centrifuges (Olander 1972).

6. Conclusions

In this paper, a source–sink stratified flow within a rapidly rotating container has been examined, and a method for computing the temperature distribution within the annular region has been developed for a wide range of thermal (ϵ_T) and fluid (ϵ_f) Rossby numbers. The temperature distribution in the container has been shown to be strongly influenced by the placement and temperature of the sources and sinks in addition to the relative magnitudes of ϵ_f and ϵ_T. Heat-transfer rates may be evaluated from the numerical solutions; at the end walls the heat-transfer rates are increased by increasing λ or for increased source temperatures. Heat-transfer rates at the side walls are generally increased with increased λ. The present analysis applies to a wide variety of source–sink geometries, and can readily be extended to consider the case of slots having an $O(1)$ height with a distributed flow and temperature distribution (Conlisk & Walker 1981).

Finally, it is of interest to discuss the relation of the present analysis to the problem of centrifugation. In a gas centrifuge, the motion of a strongly compressed gas must be considered, and the Boussinesq approximation is not valid; however, the basic structure of the flow is similar to that discussed here, and the present analysis provides an insight into the nature of the temperature field with a source–sink flow. The types of fluid motion that have been discussed here may apply to a liquid centrifuge where a separation of a binary liquid mixture is required (Svedberg & Pederson 1940; McCall & Potter 1973; Birnie & Rickwood 1978; Fujita 1975); in this case, the overall density variations are small, as is required for a Boussinesq analysis to be valid.

REFERENCES

Abramowitz, M. & Stegun, I. A. 1965 *Handbook of Mathematical Functions*, chap. 25. Dover.

Barcilon, V. & Pedlovsky, J. 1967 *J. Fluid Mech.* **29**, 673–690.

Bennetts, D. A. & Hocking, L. M. 1973 *Proc. R. Soc. Lond.* A **333**, 469–489.

Bennetts, D. A. & Jackson, W. D. N. 1974 *J. Fluid Mech.* **66**, 684–705.

Birnie, C. D. & Rickwood, D. 1978 *Centrifugal Separations in Molecular and Cell Biology*. Butterworths.

Conlisk, A. T. 1978 Ph.D. thesis, Purdue University.

Conlisk, A. T. & Walker, J. D. A. 1981 *Q. J. Mech. Appl. Math.* **34**, 89–109.

Foster, M. R. 1972 *J. Fluid Mech.* **53**, 647–655.

Fujita, H. 1975 *Foundations of Ultracentrifugal Analysis*. Wiley.

Greenspan, H. P. 1968 *The Theory of Rotating Fluids*, chapter 2. Cambridge University Press.

Hide, R. 1968 *J. Fluid Mech.* **32**, 737–764.

Homsy, G. M. & Hudson, J. L. 1969 *J. Fluid Mech.* **35**, 33–52.

Hunter, C. 1967 *J. Fluid Mech.* **27**, 753–778.

McCall, J. S. & Potter, B. J. 1973 *Ultracentrifugation*. Baillière Tindall.

Matsuda, T., Sakurai, T. & Takeda, H. 1975 *J. Fluid Mech.* **67**, 197–208.

MATSUDA, T. & HASHIMOTO, K. 1976 *J. Fluid Mech.* **78**, 337–354.
MATSUDA, T., HASHIMOTO, K. & TAKEDA, H. 1976 *J. Fluid Mech.* **73**, 389–399.
NAKAYAMA, W. & USUI, S. 1974 *J. Nucl. Sci. Tech.* **11**, 242–262.
OLANDER, D. R. 1972 *Adv. Nucl. Sci. Tech.* **6**, 105–174.
ROSSER, J. B. 1968 *Mathematics Research Center, Madison, Wisconsin, TSR* no. 797.
SPIEGEL, E. A. & VERONIS, G. 1960 *Astrophys. J.* **131**, 442–447.
STEWARTSON, K. 1957 *J. Fluid Mech.* **3**, 17–26.
SVEDBERG, T. & PEDERSEN, K. O. 1940 *The Ultracentrifuge.* Oxford University Press.